EASR

Engineering and Applied Science Research

https://www.tci-thaijo.org/index.php/easr/index

Published by the Faculty of Engineering, Khon Kaen University, Thailand

Ceria-modified zeolite: A dual-function approach for effective removal of arsenite from polluted water sources

Suttikorn Suwannatrai[1, 2], Visanu Tanboonchuy*[1, 3], Dickson Yuk-Shing Yan[4], Ratthiwa Deewan[2] and Pummarin Khamdahsag[5]

[1]Department of Environmental Engineering, Faculty of Engineering, Khon Kaen University, Khon Kaen, Thailand
[2]School of Occupational Health and Safety, Faculty of Public Health, Vongchavalitkul University, Nakhon Ratchasima, Thailand
[3]Research Center for Environmental and Hazardous Substance Management (EHSM), Khon Kaen University, Khon Kaen, Thailand
[4]Faculty of Science and Technology, The Technological and Higher Education Institute of Hong Kong, New Territories, Hong Kong
[5]Sustainable Environment Research Institute, Chulalongkorn University, Bangkok, Thailand

Received 22 April 2025
Revised 6 August 2025
Accepted 14 August 2025

Abstract

As a carcinogen, arsenic poses a significant threat when it contaminates water sources and agricultural products. In water-based environmental contamination, the most significant arsenic species are arsenate (As(V)) and arsenite (As(III)), with the latter presenting a greater challenge for removal. The development of more efficient adsorbents to successfully remove As(III) from contaminated water is still needed. A novel nanosorbent, ceria supported on Na-P zeolite (CeZ), was created in this study to perform the dual functions of oxidizing As(III) to As(V) and subsequently adsorbing the resulting As(V). CeZ was characterized by XRD, TEM, FTIR, pHpzc, and XANES analyses. Batch adsorption experiments indicated that As(III) removal in the pH range of 3-10 was highly efficient, with a maximum removal capacity of 31.746 mg g^{-1}, which was best explained by pseudo-second-order kinetics. XANES analysis confirmed that CeZ oxidized As(III) to As(V) on the surface during As(III) adsorption. The hydroxyl groups at the CeZ interface play a key role in As(III) sorption, forming inner-sphere monodentate and bidentate complexes. As(III) removal was effective because the sorption reaction was coupled with the oxidation process. Specifically, the CeO_2 on the Na-P zeolite surface was the main factor responsible for the oxidation of As(III) to As(V) and its sorption. The As(V) in the solution subsequently adsorbed onto the zeolite.

Keywords: Adsorption, Arsenite, Cerium oxide, Nanomaterials, Zeolite

1. Introduction

Arsenic (As) is a carcinogenic and poisonous element that is considered one of the most serious global environmental problems [1]. Chronic ingestion of As causes cancers of the lung, bladder, and skin as As accumulates and becomes concentrated in the lung, liver, kidney, and skin tissues, especially as a result of drinking water consumption. The WHO set a stringent standard of 10 µg L^{-1} as the acceptable amount of As in potable water [2]. The most common forms of arsenic found in ground and surface water are inorganic arsenite (As(III)) and arsenate (As(V)), respectively [3]. Compared with As(V), As(III) is more poisonous, more mobile, and more soluble in the environment [4, 5]. Therefore, the development of a rapid and efficient method for As removal, especially for As(III), is needed. Various methods have been used to remove As from drinking water, including adsorption, membrane separation, coagulation, and precipitation. Among these techniques, adsorption is one of the most common because of its low consumption requirements, high efficiency, and cost effectiveness [6]. However, the removal efficiency for As(III) is currently lower than that for As(V). Thus, the pre-oxidation of As(III) to As(V) before the adsorption process is a potential strategy for conventional As(III) treatment [7]. This common method usually requires an oxidizing agent before co-precipitation and adsorption, which increases operational costs and ancillary pollution problems [8]. Therefore, the development of an adsorbent for the efficient and cost-effective removal of As(III) that does not require a pre-oxidation process would be ideal. Recent research has extensively explored the effectiveness of potential adsorbents such as iron (Fe) nanoparticles, zero-valent iron (ZVI), iron oxide nanoparticles (IONPs), and Fe(III)-modified montmorillonite for removing As species [9-12].

Cerium oxide (CeO_2) has also been successful in removing both As(III) and As(V) [13]. Studies have shown that high As(III) removal efficiency occurs at pH 3-11 [14, 15]. It was posited that the presence of hydroxyl groups on the particles was responsible for their excellent performance. For example, Li et al. [14] used hydrous cerium oxide nanoparticles for both As(III) and As(V) adsorption. The As adsorption capacity was greater than 170 mg g^{-1} for As(III) and 107 mg g^{-1} for As(V) at neutral pH [14]. However, CeO_2 adsorbents can easily aggregate into larger particles, leading to a decreased As adsorption capacity. To prevent nanoparticle aggregation and maximize the adsorption capacity by utilizing small particles, a dispersing agent is desirable. Na-P zeolite, with its proven ability to remove As(V) (≥ 60%) via negative surface charges or cation exchange capacity (CEC), is a potential candidate [16]. However, zeolite is ineffective for As(III) removal. Therefore, one proposal is to use zeolite to mitigate the aggregation problems of CeO_2, while

*Corresponding author.
Email address: visanu@kku.ac.th
doi: 10.14456/easr.2025.56

taking full advantage of CeO_2 oxidation to eliminate As(III) [17]. However, the application and performance of CeO_2 modified with zeolite and the possibility of oxidation during As adsorption have yet to be studied. In the present work, the suitability of Na-P zeolite-supported CeO_2 (CeZ) for the removal of high concentrations of As(III) was investigated via characterization and determination of its adsorption performance.

The objective of this research was to modify CeO_2 doped on Na-P zeolite for arsenite removal. Fourier transform infrared spectroscopy (FTIR), field-emission transmission electron microscopy (FE-TEM), X-ray diffraction (XRD), point of zero charge (pH_{pzc}), specific surface area determination via the Brunauer-Emmett-Teller method (BET) method, and X-ray absorption near-edge structure spectroscopy (XANES) were used to characterize the fresh and spent CeZ to identify the composition, properties, and structure of CeZ, as well as understand As(III) removal mechanisms.

2. Methodology

2.1 Materials and preparation

Only analytical-grade chemicals, including 99% $Ce(NO_3)_3 \cdot 6H_2O$ (Merck) and NaOH (Merck), were used for CeO_2 nanoparticle synthesis in this study. The fly ash used as the raw material in this study was obtained from a coal-fired power plant in Thailand. Na-P zeolite synthesis was carried out via the Chansiriwat method [18-20]. To prepare solution A, 30.25 g of distilled water was mixed with 10 g of NaOH and 16.86 g of fly ash and heated at 100°C. Then, 10 g of solution A was mixed with 5.61 g of NaOH in 61.20 g of distilled water to form the seed gel. Solution B (mother gel) was prepared by mixing 75.00 g of distilled water with 8.27 g of NaOH and 7.98 g of fly ash, which was also heated at 100°C. The seed gel and mother gel were then combined and stirred continuously for 30 minutes. The resulting mixture was transferred into a Teflon-lined stainless-steel autoclave and subjected to hydrothermal treatment at 105 °C for 12 hours. The final product was recovered via centrifugation.

The As(III) stock solution for the adsorption experiments was prepared by dissolving $NaAsO_2$ (Merck). The RO water used to prepare all of the chemical solutions had a conductivity of 1.178 μS cm^{-1}.

CeZ was synthesized through co-precipitation by dissolving 3.1 g of $Ce(NO_3)_3 \cdot 6H_2O$ in 10 mL of RO water and 1 g of Na-P zeolite in 50 mL of 1 M NaOH [21]. The solution was stirred for 30 min at room temperature (~25°C), and then the precipitates were collected via centrifugation and washed multiple times with RO water to eliminate residual ions. The precipitates were then dried at 105°C and subsequently calcined at 250°C overnight in a furnace. The dried CeZ flakes was ground, and CeZ powder was finally obtained.

2.2 Characterization

The chemical compositions were analyzed using energy dispersive X-ray fluorescence (XRF) (MESA-50). The crystal structures of Na-P zeolite, CeO_2, and CeZ were characterized by XRD (D8 Discover, Bruker AXS). The XRD patterns were recorded in the 2θ range of 20-80° using Cu Kα radiation (λ = 0.1514 nm) at an operating voltage and current of 40 kV and 40 mA, respectively. The morphology and nanostructure of CeZ were determined by FE-TEM (JEM-3100(HR)) operated at 100 kV. The FTIR spectra were measured on a Tensor 27 FTIR spectrometer from Bruker in the range of 4000-400 cm^{-1}. The specific surface areas of CeO_2 and CeZ were measured by a nitrogen adsorption-desorption instrument (TriStar II 3020, Micromeritics) via the BET method.

The point of zero charge (pH_{pzc}) of the adsorbent was measured to determine the net surface charge of the ion in solution. The pH_{pzc} was determined by the salt addition method. In this procedure, 40 mL of DI water was adjusted to various pH values (2-11) in closed flasks. After 0.1 g of adsorbent was added to each flask, the flasks were agitated for 48 h, and the final pH was measured [22].

The oxidation states of the As and Ce complexes on the CeZ surface were measured and analyzed using As K-edge and Ce L3-edge XANES at the Synchrotron Light Research Institute (SLRI), Thailand. Au^0 and V^0 foils and As(III), As(V), Ce(III), and Ce(VI) standards were used as references. All the analyses were performed in fluorescence and transmission modes via a 19-element Ge detector.

2.3 Batch adsorption experiments

Kinetic experiments were conducted in a 600 mL beaker containing 500 mL of 10 mg L^{-1} As(III) solution and adsorbents. The dosage of adsorbents for As(III) was 10 mg L^{-1}. For the adsorption experiments, beakers containing As solution and adsorbents were stirred at 160 rpm at room temperature (27°C) for 6 h and conducted at a pH of 7.5±0.5.

The effect of pH on As(III) adsorption was examined by varying the pH range from 3 to 10. The solutions' pH was adjusted by adding NaOH and HCl. The contact time was determined after the kinetic experiment.

Adsorption isotherm experiments were conducted in a 50 mL centrifuge tube containing 50 mL of As(III) solution. The materials were added to As(III) solutions with initial concentrations of 1 to 50 mg L^{-1}. Subsequently, the solutions were shaken with a vertical rotating mixer at 160 rpm at room temperature. After adsorption, the samples were filtered from the solution using a 0.45 μm syringe filter and collected to measure the concentrations of As via an inductively coupled plasma optical emission spectrometer (ICP-OES, PerkinElmer Optima 8000).

3. Results and discussion

3.1 Material characterizations

The major elements of fly ash and zeolite were measured by XRF and are represented as the main oxides of SiO_2, Al_2O_3, some amount of Fe_2O_3, and other oxides (Table 1). The results revealed that the materials contained high contents of SiO_2 in raw fly ash, Na-P, Na-P (C), and Na-P (K) with SiO_2/Al_2O_3 ratios of 3.44, 2.22, 1.90, and 2.39, respectively. After zeolite synthesis, the Si/Al ratio was reduced from 3.44 to 2.22, corresponding to previous research, in which synthesized Na-P zeolite obtained ratios of Si/Al between 1.90 and 2.39.

Table 1 Chemical composition of the used fly ash and synthesized Na-P as revealed by the XRF technique

Sample	X-ray fluorescence analyses, wt%									Ref.
	SiO_2	Al_2O_3	Fe_2O_3	CaO	K_2O	MgO	Na_2O	LOI	Si/Al	
Fly ash	59.46	17.27	4.56	11.73	1.36	0.96	0.73	2.37	**3.44**	This study
Na-P	42.35	19.00	6.55	9.30	1.58	1.33	14.82	6.07	**2.22**	This study
Na-P (C)	32.35	17.00	16.55	22.30	0.58	1.33	7.82	2.07	**1.90**	[18]
Na-P (K)	63.10	26.30	0.90	1.10	0.60	1.50	5.50	1.00	**2.39**	[23]

The crystal structures of Na-P zeolite, CeO_2, and CeZ were characterized by XRD, and their XRD patterns are shown in Figure 1a. The characteristic peaks of the Na-P zeolite pattern can be noted at approximately 2θ = 26.7, 28.2, 29.5, and 33.5 degrees (JCPDS 40-1464). The face-centered-cubic (FCC) structure of the CeO_2 pattern is notable at approximately 2θ = 28.5, 33.0, 47.4, 56.3, 59.3, 69.6, 76.7, and 79.1 degrees (JCPDS 00-034-0394), confirming the synthesis of pure phase CeO_2. The XRD pattern of CeZ showed identical peaks for all three substances. However, some substantial loss of CeO_2 crystallinity occurred (XRD patterns at around 2θ = 47.4, 56.3, and 69.6 degrees, corresponding to the 220, 311, and 222 crystalline planes, respectively). Thus, CeO_2 was observed in the CeZ, indicating the successful fabrication of the targeted materials.

TEM was used to study the morphology and microstructure of the CeZ. The CeZ consisted of ultrafine nanoparticles with a relatively uniform size of around 3.5 nm on average (Figure 1b), indicating that zeolite can serve as a deterrent to the aggregation of CeO_2 into large particles. Moreover, the typical lattice fringe spacing was measured to be 0.29 nm and corresponded to the (111) plane spacing of CeO_2, which was consistent with previous XRD research [8].

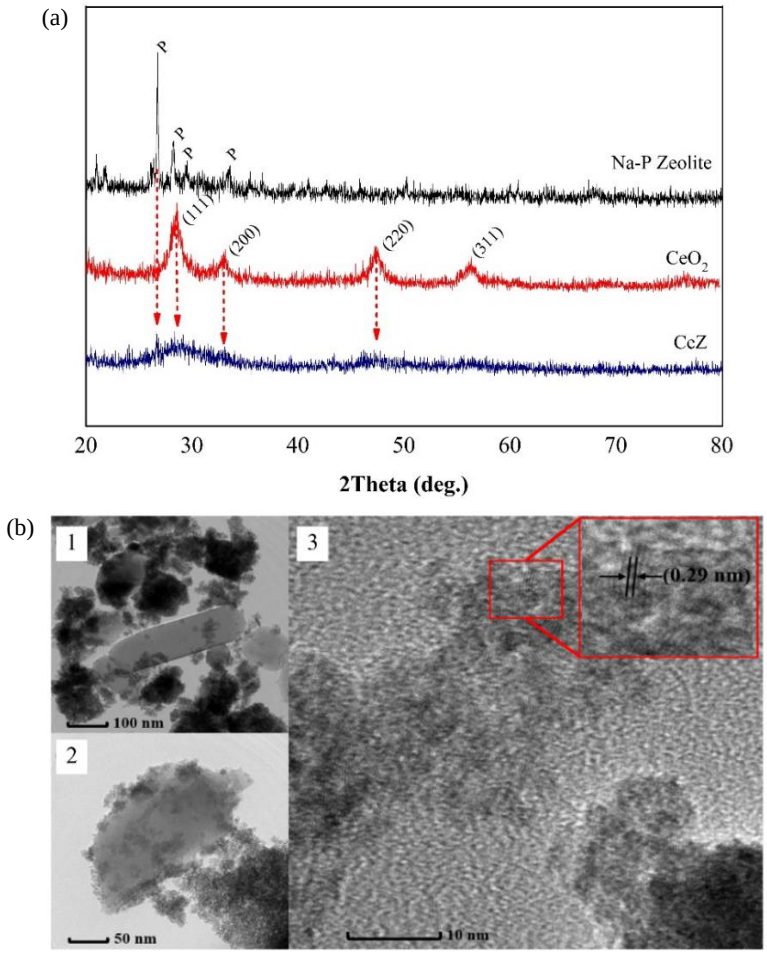

Figure 1 (a) XRD patterns and (b) TEM images of CeZ with magnification 10 nm, 50 nm, and 100 nm with a lattice spacing of the (111) plane of CeO_2.

The FTIR spectra of the CeO_2 and CeZ are presented in Figure 2a. The peak at 3418 cm^{-1} was revealed in the CeO_2 and CeZ spectra, indicating -OH stretching and bending vibration modes [19]. However, the percent transmittance of CeZ decreased compared with that of CeO_2 implying that the number of -OH groups on the material surface decreased. Strong and broad bands at 1632-1622 cm^{-1} (O-H out-of-plane bend) and 1079-1053cm^{-1} (C-OH stretching vibration) were present in the CeO_2 and CeZ. Moreover, two new peaks at 996 and 537 cm^{-1} were found as the stretching of the CeO-O band after the CeO_2 was doped with zeolite. It was concluded that the functional groups of -OH and C-OH could play a role in the As(III) adsorption reaction over CeZ. Our investigation into the possible adsorption mechanisms of As(III) removal by CeO_2 had similar findings and are discussed in Section 3.5.

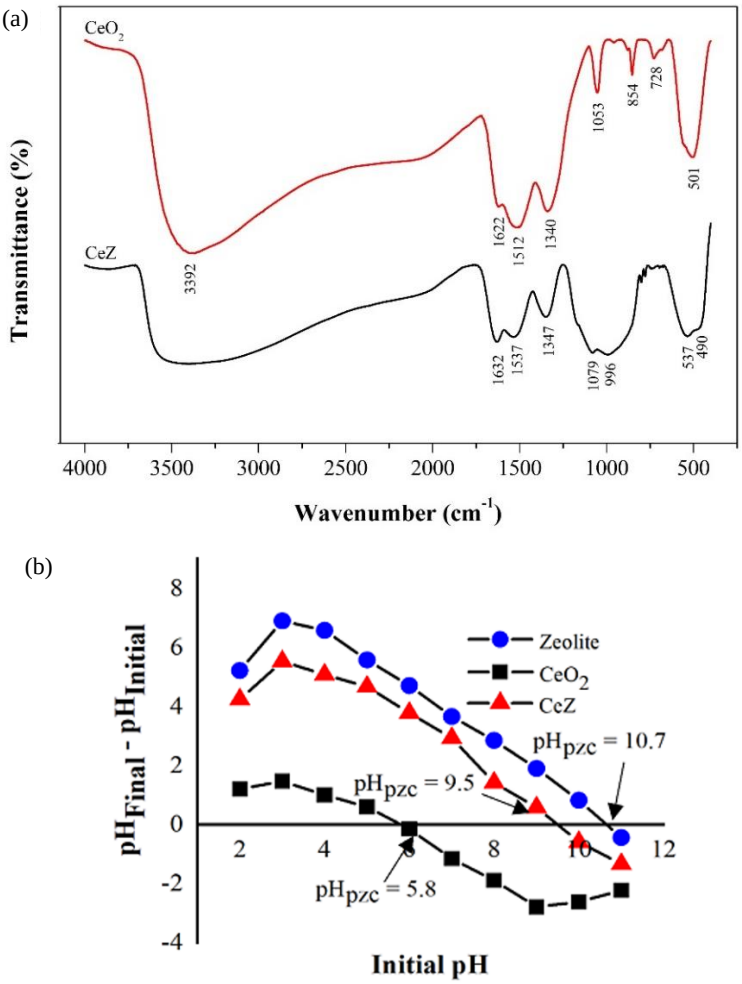

Figure 2 (a) FTIR spectra of CeO_2 and CeZ at calcination temperature of 250 °C and (b) Plot of initial pH versus final pH for determination of pH_{pzc}.

The pH_{pzc} values of ash, zeolite, CeZ, and CeO_2 were found to be 11.0, 10.3, 9.5, and 6.0, respectively (Figure 2b). The pH_{pzc} of CeZ was at a higher pH compared to that of CeO_2 but at a lower pH compared to that of zeolite. This result was probably caused by the composition of CeO_2 and zeolite in the CeZ. The adsorbent surface is positively charged at $pH < pH_{pzc}$, which favors anions, and is negatively charged at $pH > pH_{pzc}$, which benefits adsorbing cations [24].

Therefore, the role of pH in As speciation is important, since As(III) species, such as H_3AsO_3 and H_2AsO^{3-} at pH < 9.2 and AsO^{2-} at pH > 9.2, dominate these conditions, whereas H_2AsO^{4-}, $HAsO_4^{2-}$ and AsO_4^{3-} are the dominant As(V) species in the pH ranges of 2-6, 6-11, and 11-14, respectively [25]. The pH_{pzc} of 9.5 indicated that CeZ would have a positive surface charge at pH < 9.5 and would therefore be likely to attract As(III) ($As(OH)_3$ and $AsO(OH)_2^-$) and transform As(V) ($AsO_2(OH)_2^-$ and $AsO_3(OH)_2^-$). The pH_{pzc} of CeZ composite materials is a result of complex surface interactions between CeO_2 nanoparticles and zeolite. When CeO_2 is added, its amphoteric surface sites (donating/accepting protons) combine with the negatively charged aluminosilicate network of the zeolite, leading to simultaneous surface phenomena. The overall pH_{pzc} depends on the abundance and accessibility of these sites. Experiments have shown that increasing the CeO_2 content shifts the pH_{pzc} to more acidic values. This is likely due to Ce–OH functional groups, which have different acid-base properties than the Si–OH and Al–OH groups in pure zeolite. Therefore, the CeO_2-to-zeolite ratio is crucial for the overall surface charge of a composite.

The specific surface areas of CeO_2 and CeZ were calculated to be 58.4 and 224.6 $m^2\ g^{-1}$, respectively, according to the BET method. Therefore, the zeolite increased the surface area, which should improve the As removal capacity.

3.2 Batch adsorption studies

The initial pH of a solution is known to affect the adsorption process. In our study, As(III) sorption by CeZ decreased slightly with increasing solution pH and reached its maximum in the pH range of 3-7 (Figure 3a). At a relatively high pH, As(III) sorption decreased slightly. Adsorption of weak acid anions over metal oxides is typically maximized at a pH close to the pKa_1 of the acid, which is 9.2 for arsenious acid. The decrease in As(III) sorption may be attributable to the coulombic repulsion between As(III) forms and the decreased charge of the CeZ surface [26].

The Variation of C/C_0 by CeO_2 and CeZ versus time is shown in Figure 3b. The As(III) removal of each sorbent occurred rapidly in the first 120 min and then continued slowly thereafter. As(III) removal by CeZ was slightly better than that by CeO_2, indicating that the zeolite was helpful as a protective agent against CeO_2 aggregation, a result that was consistent with the TEM results. The Na-P zeolite was also able to continue removing As over time (Figure 3b).

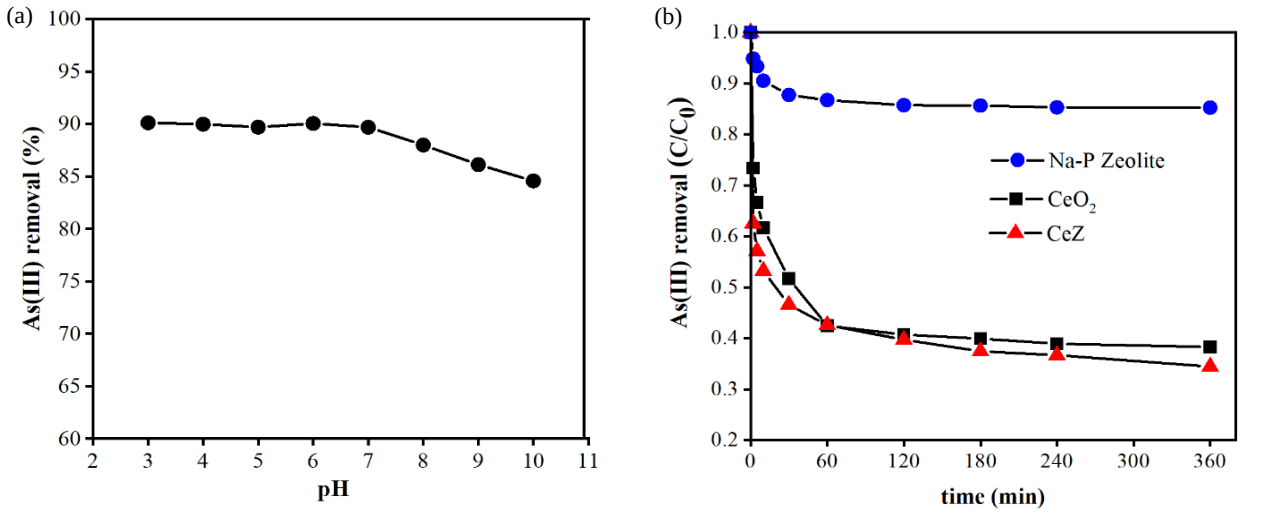

Figure 3 (a) Effect of pH at 120 min on As(III) sorption for CeZ and (b) comparison of As(III) sorption at pH 7.5 ±0.5 for three different materials (initial As(III) concentration of 10 mg L^{-1} and sorbent loading of 0.5 g L^{-1}).

Table 2 Kinetic model and adsorption isotherm parameters evaluated for the sorption of As(III) by CeO_2 and CeZ.

Model	Equation	Parameter, unit	CeO	CeZ
2nd–order	$\frac{t}{q_t}=\frac{1}{k_2 q_e^2}+\frac{1}{q_e}t$	k_2, g mg^{-1} min^{-1}	0.003	0.003
		$q_{e,cal}$, mg g^{-1}	65.34	68.49
		R^2	0.999	0.999
Intraparticle	$q_t = k_i t^{0.5}$	k_1, mg g^{-1} $(min^{0.5})^{-1}$	4.983	3.177
		R^2	0.986	0.948
		k_2, mg g^{-1} $(min^{0.5})^{-1}$	0.391	0.755
		R^2	0.968	0.980
Langmuir	$\frac{C_e}{q_e}=\frac{1}{K_L q_m}+\frac{C_e}{q_m}$	q_m, mg g^{-1}	-	31.75
		K_L, L g^{-1}	-	1.981
		R^2	-	0.904
Freundlich	$\ln(q_e) = \ln(K_f) + \left(\frac{1}{n}\right)\ln(C_e)$	K_F, (mg g^{-1}) (L $mg^{-1})^{-1/n}$	-	15.74
		n	-	2.848
		R^2	-	0.994
D-R	$\ln(q_e)=\ln(q_e)-(k\varepsilon^2)$	q, mol g^{-1}	-	549.6
	$\varepsilon = RT\ln\left(+1\frac{1}{C_e}\right)$	E, J mol^{-1}	-	13.61
	$E=\frac{1}{\sqrt{2k_{DR}}}$	R^2	-	0.983
Temkin	$q_e = B\ln A + C_e$	B_T, J mol^{-1}	-	8.377
		A, K_T, L g^{-1}	-	8.829
		R^2	-	0.928

3.3 Adsorption kinetic study

Kinetics data describing the adsorption reaction were analyzed using pseudo-first -order (Eq. 1) and pseudo-second-order (Eq. 2) models, expressed as follows [26]:

$$\log\left(q_e - q_t\right) = \log q_e - \frac{k_1 t}{2.303} \quad (1)$$

$$\frac{t}{q_t}=\frac{1}{k_2 q_e^2}+\frac{t}{q_e} \quad (2)$$

where q_t and q_e (mg g^{-1}) are the amounts of As(III) sorption at time t (min) and at equilibrium, respectively, and k_1 (min^{-1}) and k_2 (g mg^{-1} min^{-1}) are the rate constants for Eqs. 1 and 2, respectively.

The kinetic parameters obtained from the fitted data in Figure 4a are summarized in Table 2. To better understand the reaction kinetics of As(III) removal by CeO2 and CeZ, pseudo-second order kinetics were applied to the experimental data. The model fit was evaluated using the correlation coefficient (R^2). Consequently, the mechanism of As adsorption on CeZ appears to be chemisorption, driven by valence forces and characterized by the sharing or exchange of electrons between CeO_2, zeolite, and As(III). A comparison between CeO_2 and CeZ showed that the removal efficiency of CeZ at 120 min was higher than that of CeO_2.

The mathematical correlation between the concentration of the adsorbed substance on the solid surface and $t^{0.5}$ was derived by analyzing the adsorption mechanism governed by intraparticle diffusion within the adsorbent (Eq. 3).

$$q_t = k_{id} t^{0.5} + C_{id} \quad (3)$$

where k_{id} is the intraparticle diffusion rate constant (mg g^{-1} $min^{-0.5}$) and C_{id} is the intercept. The value of C_{id} is proportional to the boundary layer thickness. Thus, when C_{id} is zero, the rate of sorption is likely controlled by intraparticle diffusion. However, the plot of q_t versus $t^{0.5}$ often shows multiple linear segments. If the slope of the first portion is not zero, then the sorption is initially controlled by film diffusion. Thus, the value of the intercept provides an idea about the thickness of the boundary layer. The larger the intercept is, the greater the boundary layer effect. The results suggested that adsorption occurred in two phases (Figure 4b). First, film diffusion occurred, as shown by the steep slope, which was later followed by a gradual adsorption stage where intraparticle or pore diffusion was rate-limiting. Because the plot did not pass through the origin, intraparticle diffusion was not the sole rate-limiting step. Instead, the adsorption rate was limited by different processes, but there was only one rate-limiting process at any particular time.

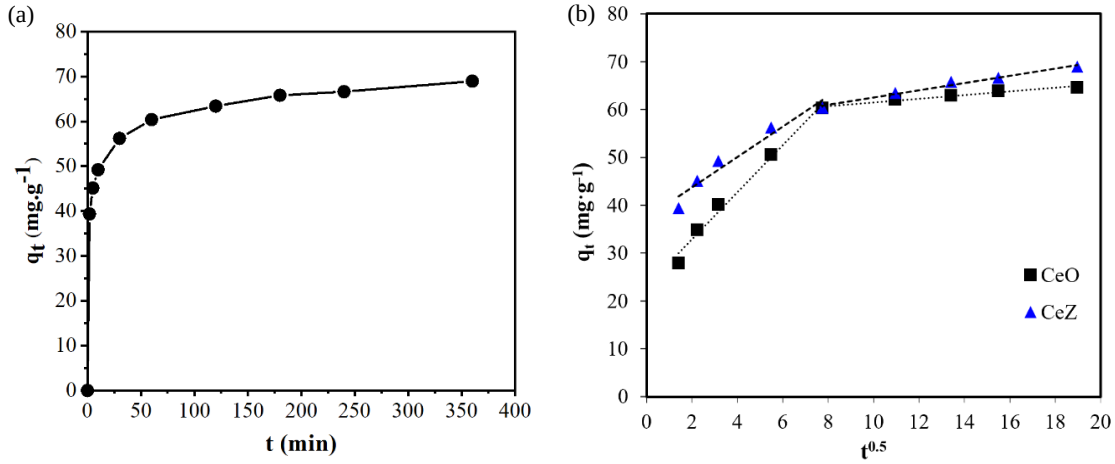

Figure 4 (a) Adsorption kinetics and (b) intraparticle diffusion model for As(III) adsorption by CeZ material (experimental conditions: initial As(III) concentration of 10 mg L^{-1}, sorbent loading 0.5 of g L^{-1}, and pH of 7.5 ±0.5).

3.4 Adsorption isotherm study

The experimental data were fitted to Freundlich and Langmuir adsorption isotherms (Eqs. (4) and (5), respectively). Equilibrium adsorption isotherm plots were used to examine As(III) adsorption capacity of CaZ (Figure 5a).

$$q_e = \frac{q_{max} K_L C_e}{1 + K_L C_e} \quad (4)$$

$$q_e = K_F C_e^{\frac{1}{n}} \quad (5)$$

where q_e (mg g^{-1}) is the amount of As(III) adsorbed by CeZ, and Ce (mg L^{-1}) at equilibrium, q_{max} (mg g^{-1}) is the maximum amount of As(III) adsorbed by CeZ, K_F (mg g^{-1}) (L $mg^{-1})^{1/n}$ is related to the adsorption capacity of CeZ, 1/n is a constant known as the heterogeneity factor that is related to surface heterogeneity, and K_L (L mg^{-1}) is a constant related to the heat of adsorption.

The R^2 for the Freundlich isotherm was also greater than that of the Langmuir isotherm (Table 2). As shown in Figure 5a, the Freundlich isotherm plot showed a relatively better fit to the experimental data than the Langmuir isotherm plot. The data for As(III) in the plot demonstrated very favorable linear correlation coefficients, implying a good fit to a linear model. Figure 5a presents the sorption isotherm for As(III), showing the concentration of As(III) in the solid phase (adsorbed by CeZ) relative to its equilibrium concentration in the leachate. The Freundlich isotherm model effectively described the adsorption of As(III) by CeZ. Furthermore, the 'n' values for As(III), which were greater than 1, confirmed that the adsorption process was favorable. According to the Freundlich model, the most important assumption is that sorption takes place on heterogeneous surfaces, both in terms of the sorption sites and the heterogeneous energy distribution among the surfaces. Moreover, it describes reversible adsorption that can form multilayers.

The data were also analyzed using the D-R isotherm (Eq. 6) in order to estimate sorption energy for As(III) [19].

$$\ln Q_e = \ln Q_m - K_{DR} \varepsilon^2 \quad (6)$$

Q_e and Q_m denote the equilibrium and saturated sorption capacities in mol kg^{-1}, respectively, whereas K_{DR} is a constant associated with the free energy (mol^2 kJ^{-2}) of sorption. The values of Q_m and K_{DR} were derived from the slope and intercept of the $\ln Q_e$ versus ε^2 plot, where ε represents the Polanyi potential, as expressed in Eq. 7:

$$\varepsilon = \ln RT\left\{1 + \frac{1}{C_e'}\right\} \quad (7)$$

where C_e' (mol L^3) denotes the same meaning as C_e as described above, and R and T are the molar gas constant (kJ mol^{-1}) and absolute temperature (K), respectively.

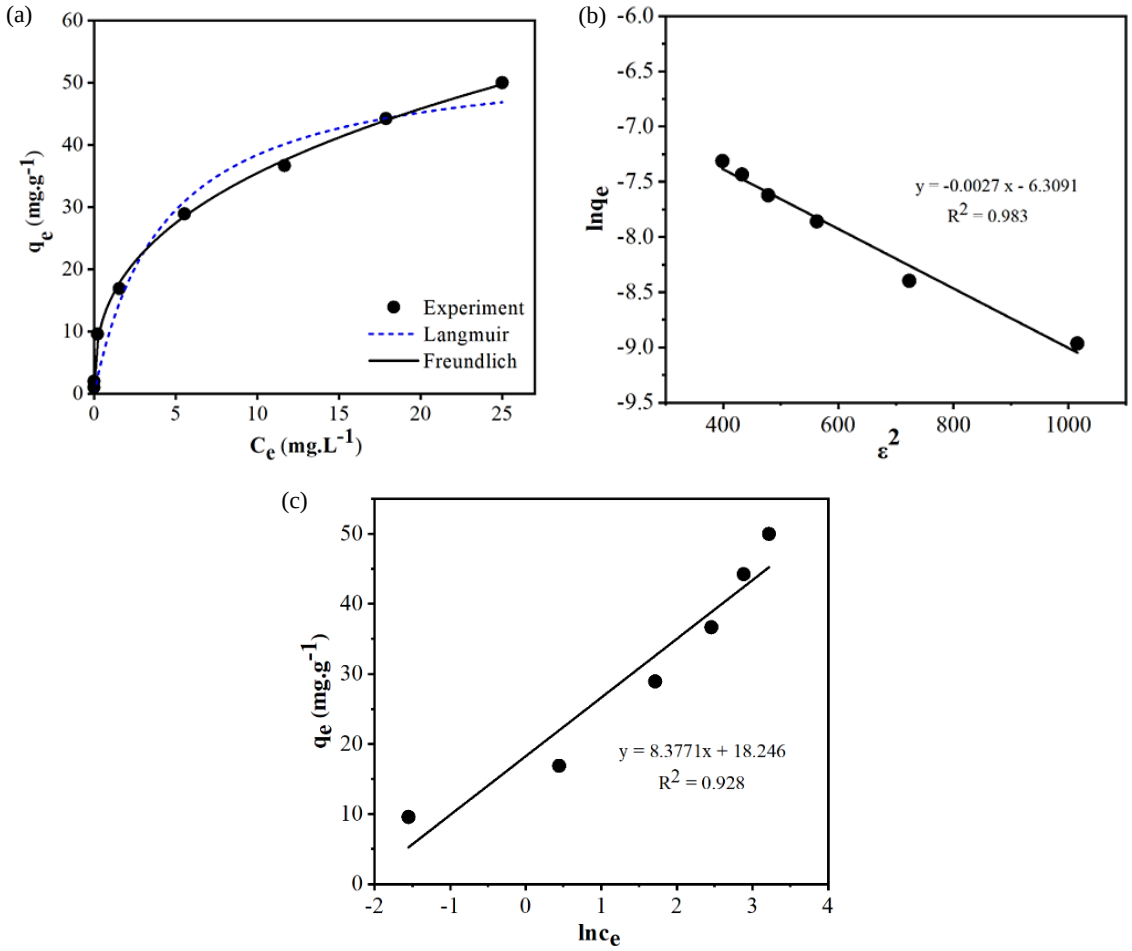

Figure 5 (a) Adsorption isotherms for As(III) adsorption by CeZ material and (b) Dubinin Radushkevich, and (c) Temkin isotherms for As(III) adsorption by CeZ material (experimental conditions: initial As(III) concentration of 10 mg L-1, sorbent loading of 0.5 g L-1, and pH of 7.5 ±0.5).

The D-R isotherm data from the fitting in Figure 5b are summarized in Table 2. The mean free energy (E) of sorption was calculated from Eq. 8, which relates the mean free energy (E, kJ mol^{-1}) of sorption to the K_{DR}.

$$E = \frac{1}{\sqrt{2K_{DR}}} \quad (8)$$

The mean free energy of sorption (E) was determined to be 2.886 kJ mol^{-1}. Because E was less than 8 kJ mol^{-1}, As(III) sorption by the CeZ sample occurred through physical adsorption processes. Physical sorption is possible and is consistent with the results of surface area and pH effects. Thus, this finding supports the theory that As(III) was oxidized to As(V) as it came into contact with the oxide surface.

The Temkin isotherm equation (Eq. (9)) assumes that as the number of coverage layers increases, the heat of adsorption of all the molecules decreases linearly due to adsorbent-adsorbate interactions. The theory also assumes that the bonding energies are uniformly distributed, up to some maximum binding energy.

$$q_e = \frac{RT}{b_T} \ln\left(k_T C_e\right) \quad (9)$$

where, R is the universal gas constant (8.314 J mol^{-1} K^{-1}), T is the absolute temperature (K), k_T is the equilibrium binding constant (L mg^{-1}) corresponding to the maximum binding energy and b_T is the variation in the adsorption energy (kJ mol^{-1}). This model can be linearized (Eq. 10) as follows (shown in Figure 5c):

$$q_e = B\ln k_T + B\ln C_e \quad (10)$$

where $B = RT/b_T$ is the Temkin constant related to the heat of adsorption (J mol^{-1}). The values of k_T and B were calculated from the intercept and the slope of the linear plot of q_e vs lnC_e. Based on the R^2 values of both isotherms (Table 2), the experimental data fit well with the D-R isotherm (R^2 = 0.983), indicating that As(III) adsorption onto CeO_2 is a physical adsorption process.

Comparisons of the removal efficiency of the prepared adsorbents with those in previous reports were difficult because of differences in procedures and experimental conditions. Nevertheless, the adsorption capacity of CeZ was compared to that of existing materials (Table 3). As(III) removal by CeZ was much higher than that achieved by the other adsorbents, except for one, in which the adsorption was reported to be 36.8 mg g^{-1} when CeO_2-modified activated carbon was used [27]. Although CeO_2-modified activated

carbon had a higher removal capacity than CeZ, a comparison of production and investment costs shows that activated carbon is more expensive than zeolite. Furthermore, CeZ has a relatively high adsorption rate and functions ideally under neutral pH conditions that are typical of surface water and groundwater contaminated by As(III).

Table 3 Comparison of adsorbents in terms of As**(III)** adsorbent capacity

Adsorbent	Surface area (m^2 g^{-1})	Adsorption capacity (mg g^{-1})	Initial As(III) conc. (mg L^{-1})	pH	Ref.
PS-350-HFO	350	11.08	5	7	[28]
PANi/PVA	-	27.25	10	11	[29]
BT-4	229	27.4	70	3	[30]
NICMO	104	2.42	4.8	7	[31]
CeO_2/AC	414.1	36.8	10	5	[32]
CeO_2	67.5	21.27	10	7-8	[13]
CeZ	224.6	31.75	10	7-8	This study

The cost of the chemicals used to synthesize 1 gram of CeZ material is $0.45. (Note that this cost varies depending on the supplier and purchase volume.) Therefore, according to Table 3, the amount of CeZ material required to treat 1 m^3 of water contaminated with 10 mg/L arsenic is 44.5 grams, which costs approximately $20.11 per 1 m^3 of water.

3.5 Mechanisms and interactions of arsenic on the CeZ surface

The normalized As K-edge XANES spectra of the reference materials were characteristic of the As(III) and As(V) standards (11870.3 and 11873.3 eV, respectively) (Figure 6a). The normalized As K-edge XANES spectra of both the CeO_2 and CeZ samples showed that the spectral properties were paired with the As(III) standard, whereas the XANES spectra of CeZ samples showed that both spectral properties were paired with the As(III) and As(V) standard. The results identified a coexistence of As(III) and As(V) on the surface of CeO_2, which is consistent with the fact that, to a certain extent, As(III) can be oxidized to As(V) on the surface of CeO_2 through the Ce(IV) redox reaction [13]. Dahle and Arai [33] noted that CeO_2 has an especially high oxygen storage capacity and can easily change between its Ce(III) and Ce(IV) states. This makes CeO_2 a superior choice as a catalyst.

In addition, the Ce L_3-edge XANES spectra of fresh and spent CeZ were analyzed. The XANES spectra for CeZ showed peaks representative of the Ce(III) standard present at 5467.40 eV and double peaks representative of the Ce(IV) standard present at 5470.60 eV and 5477.19 eV (Figure 6b). For fresh and spent CeZ, combinations of Ce(IV) and Ce(III) were identified as electron transmission between Ce(IV) and As(III), leading to a change in As(III) to As(V) on the surface, as described by Eq. 11:

$$2CeO_2 + 3H_3AsO_3 \longrightarrow H_3AsO_4 + 2CeAsO_3 + 3H_2O \quad (11)$$

There was oxidation of As(III) to As(V) by receiving electrons from the CeO_2 oxidation-reduction reaction. CeO_2 was reduced to Ce_2O_3 as a Ce(III) intermediate reaction product. This generated Ce_2O_3 that could oxidize H_3AsO_3 to H_3AsO_4 and Ce(III) was combined with As(III) in the form of $2CeAsO_3$. The results of Ce L_3-edge XANES spectra analysis suggested that CeO_2 was involved as an As species adsorbent and acted as an oxidizing agent.

Based on the XANES results, possible mechanisms for As(III) adsorption on the CeZ surface can be inferred. Previous studies have pointed to As(III) adsorption by way of hydroxyl group bonds that form on the CeZ surface (Ce-OH) after the reaction. FTIR analysis has similarly revealed that Ce-OH and -OH functional groups are involved in the As(III) ions adsorption on CeZ (CeO_2 on the surface) since highly hydroxylated As(III) complexes were formed via a reaction between Ce-OH and As-OH [8, 34-36]. Fast adsorption kinetics have indicated chemisorption related to valence forces through a sharing mechanism between CeO_2, zeolite, and As(III) [14]. Therefore, these results suggested that the mechanism of As(III) adsorption on CeZ involved the formation of inner-sphere complexes at its surface hydroxy groups. The adsorption behavior being unaffected by pH provides evidence for the complexity of the inner sphere where the As(III) species exchange with the -OH group directly coordinated with the CeZ surface. With a rapid and efficient process, monodentate and bidentate surface complexes allow CeO_2 to adsorb As(III) [6].

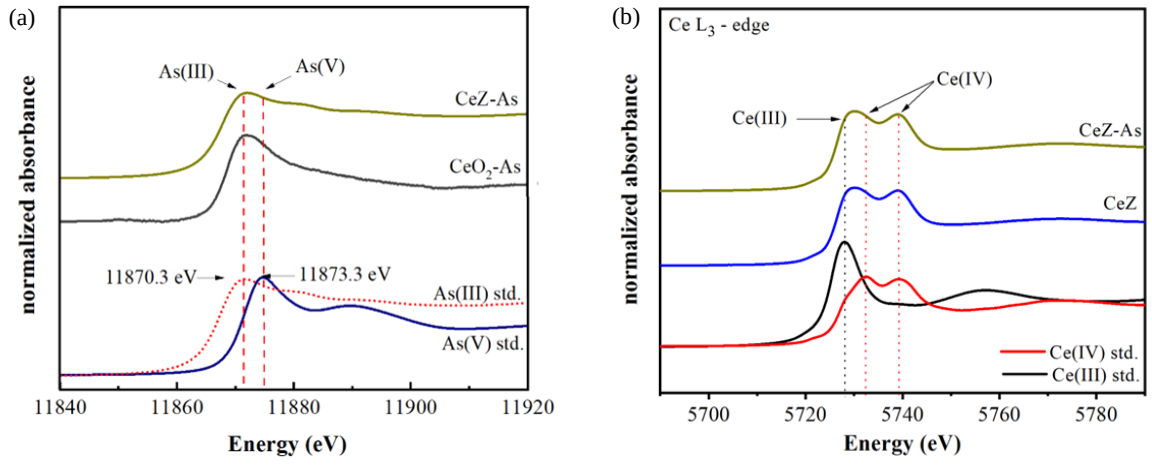

Figure 6 Normalized (a) K-edge XANES data of the CeZ-As, CeO2-As, As(III), and As(V) standards (the energy scale is relative to the As(III) and As(V) K-edge) and (b) Ce L3-edge XANES data of the CeZ-As, CeZ, Ce(IV), and Ce(III) standards (the energy scale is relative to the Ce(IV) and Ce(III) L3-edge.

The XANES method, which was used to analyze the reaction in terms of its relationship to contact time, suggested that, under experimental conditions, the As(III) on the surface of CeZ was partially transformed to As(V) via an oxidation reaction and then adsorbed over CeO_2 and the zeolite surface through two mechanisms: surface complexation and the oxidation-reduction reaction of CeO_2 to Ce_2O_3. As(III) is oxidized to As(V) by donating electrons in the oxidation-reduction reaction of CeO_2. After that, the Na-P zeolite was able to remove As(V) from the solution via the oxidation of CeO_2, as shown in Figure 7. Thus, the proposed mechanisms of As(III) adsorption over CeZ were as follows: (i) complexation between -OH groups and As(III) on the CeO_2 surface; (ii) As(III) oxidation to As(V) via an oxidation-reduction reaction; and (iii) As(V) elimination by adsorption onto the Na-P zeolite and CeO_2 surfaces. Furthermore, As(III) can adsorb by forming inner-sphere complexes with Ce(III) in the form of $CeAsO_3$.

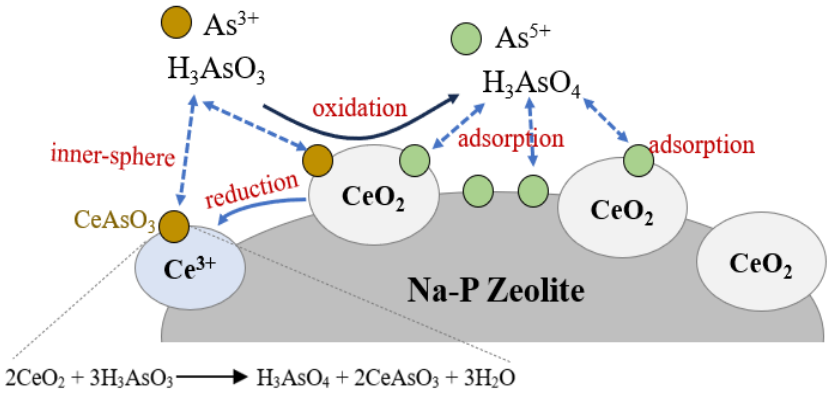

Figure 7 Proposed mechanisms and interactions of arsenic on the CeZ surface.

4. Conclusions

Our results showed that CeZ could be synthesized successfully and used in a simple adsorption process for As(III) contamination in water. The Na-P zeolite alleviated the aggregation of large particles of CeO_2 nanoparticles and allowed As(V) removal via the oxidation of CeO_2. The behavior of As(III) adsorption was consistent with the Freundlich adsorption isotherm and a pseudo-second order kinetic model. D-R and Temkin isotherms indicated that the adsorption behavior was physisorption. The XANES spectra of CeZ indicated that the oxidation states of As occurred on the interface of the spent CeZ. The mechanisms of As(III) adsorption were related to As(III) adsorption on the CeZ surface, As(III) oxidation to As(V), and the adsorption of As(V) in the solution on the surface of the material.

5. Acknowledgment

This work was supported by the Fundamental Fund (The National Science, Research and Innovation Fund (NSRF), Thailand).

6. References

[1] Xiong Y, Tong Q, Shan W, Xing Z, Wang Y, Wen S, et al. Arsenic transformation and adsorption by iron hydroxide/manganese dioxide doped straw activated carbon. Appl Surf Sci. 2017;416:618-27.
[2] Yadav R, Sharma AK, Babu JN. Sorptive removal of arsenite [As(III)] and arsenate [As(V)] by Fuller's earth immobilized nanoscale zero-valent iron nanoparticles (F-NZVI): effect of Fe^0 loading on adsorption activity. J Environ Chem Eng. 2016;4(1): 681-94.
[3] Panda AP, Jha U, Swain SK. Synthesis of nanostructured copper oxide loaded boehmite (CuO_Boehmite) for adsorptive removal of As(III/V) from aqueous solution. J Water Process Eng. 2020;37:101506.
[4] Cheng Z, Fu F, Dionysiou DD, Tang B. Adsorption, oxidation, and reduction behavior of arsenic in the removal of aqueous As(III) by mesoporous Fe/Al bimetallic particles. Water Res. 2016;96:22-31.
[5] He Z, Senlin T, Ping N. Adsorption of arsenate and arsenite from aqueous solutions by cerium-loaded cation exchange resin. J Rare Earths. 2012;30(6):563-72.
[6] Liu D, Deng S, Maimaiti A, Wang B, Huang J, Wang Y, et al. As(III) and As(V) adsorption on nanocomposite of hydrated zirconium oxide coated carbon nanotubes. J Colloid Interface Sci. 2018;511:277-84.
[7] Nidheesh PV, Divyapriya G, Cerkez EB, Gopinath A, Banerji T, Strongin DR. Oxidative sorption of arsenite from water by iron: a mechanistic perspective. Environ Sci: Water Res Technol. 2022;8:2466-90.
[8] Zhang L, Zhu T, Liu X, Zhang W. Simultaneous oxidation and adsorption of As(III) from water by cerium modified chitosan ultrafine nanobiosorbent. J Hazard Mater. 2016;308:1-10.
[9] Tanboonchuy V, Hsu JC, Grisdanurak N, Liao CH. Impact of selected solution factors on arsenate and arsenite removal by nanoiron particles. Environ Sci Pollut Res. 2011;18:857-64.
[10] Neisan RS, Saady NMC, Bazan C, Zendehboudi S, Venkatachalam P. Use of mussel shells for removal of arsenic from water: kinetics and equilibrium experimental investigation. Results Eng. 2025;25:103587.
[11] Deewan R, Yan DYS, Khamdahsag P, Tanboonchuy V. Remediation of arsenic-contaminated water by green zero-valent iron nanoparticles. Environ Sci Pollut Res. 2023;30:90352-61.
[12] Deewan R, Tanboonchuy V, Khamdahsag P, Yan DYS. Utilization of agricultural waste: mango peels and pineapple crown leaves as precursors for nanomaterial production for arsenate remediation. Environ Sci Pollut Res. 2025;32:14508-26.
[13] Suwannatrai S, Yan DYS, Phanthasri J, Khamdahsag P, Wannapaiboon S, Tanboonchuy V. Oxidation-adsorption of arsenite contaminated water over ceria nanorods. Desalin Water Treat. 2020;200:252-61.

[14] Li R, Li Q, Gao S, Shang JK. Exceptional arsenic adsorption performance of hydrous cerium oxide nanoparticles: part A. Adsorption capacity and mechanism. Chem Eng J. 2012;185-186:127-35.
[15] Nakseedee P, Tanboonchuy V, Khemthong P, Grisdanurak N, Liao CH. Role of Cu on zero valent bimetallic Cu-Fe in arsenic removal with gas bubbling. Environ Prog Sustain Energy. 2017;36(5):1449-57.
[16] Li Z, Beachner R, McManama Z, Hanlie H. Sorption of arsenic by surfactant-modified zeolite and kaolinite. Microporous Mesoporous Mater. 2017;105(3):291-7.
[17] Li Z, Wang L, Meng J, Liu X, Xu J, Wang F, et al. Zeolite-supported nanoscale zero-valent iron: new findings on simultaneous adsorption of Cd(II),Pb(II), and As(III) in aqueous solution and soil. J Hazard Mater. 2018;344:1-11.
[18] Chansiriwat W, Tanangteerapong D, Wantala K. Synthesis of zeolite from coal fly ash by hydrothermal method without adding alumina and silica sources: effect of aging temperature and time. Sains Malaysiana. 2016;45(11):1723-31.
[19] Phanthasri J, Grisdanurak N, Khamdahsag P, Wantala K, Khunphonoi R, Wannapaiboon S, et al. Role of zeolite-supported nanoscale zero-valent iron in selenate removal. Water Air Soil Pollut. 2020;231:199.
[20] Phanthasri J, Yan DYS, Wantala K, Khunphonoi R, Tanboonchuy V. Reduction and adsorption co-processes for selenate removal by zeolite-supported nanoscale zero-valent iron. Eng Appl Sci Res. 2022;49(3):363-72.
[21] Singh LH, Pati SS, Coaquira JAH, Matilla J, Guimaraes EM, Oliveira AC, et al. Magnetic interactions in cubic iron oxide magnetic nanoparticle bound to zeolite. J Magn Magn Mater. 2016;416:98-102.
[22] Hassan AF, Elhadidy H. Production of activated carbons from waste carpets and its application in methylene blue adsorption: kinetic and thermodynamic studies. J Environ Chem Eng. 2017;5(1):955-63.
[23] Kazemian H, Naghdali Z, Kashani TG, Farhadi F. Conversion of high silicon fly ash to Na-P1 zeolite: alkaline fusion followed by hydrothermal crystallization. Adv Powder Technol. 2010;21(3):279-83.
[24] Gupta K, Bhattacharya S, Nandi D, Dhar A, Maity A, Mukhopadhyay A, et al. Arsenic(III) sorption on nanostructured cerium incorporated manganese oxide (NCMO): a physical insight into the mechanistic pathway. J Colloid Interface Sci. 2012;377(1): 269-76.
[25] Cheng S, Zhang L, Ma A, Xia H, Peng J, Li C, et al. Comparison of activated carbon and iron/cerium modified activated carbon to remove methylene blue from wastewater. J Environ Sci. 2018;65:92-102.
[26] Shehzad K, Xie C, He J, Cai X, Xu W, Liu J. Facile synthesis of novel calcined magnetic orange peel composites for efficient removal of arsenite through simultaneous oxidation and adsorption. J Colloid Interface Sci. 2018;511:155-64.
[27] Dubey S, Banerjee S, Upadhyay SN, Sharma YC. Application of common nano-materials for selected metallic species from water and wastewaters: a critical review. J Mol Liq. 2017;240:656-77.
[28] Wang J, Zhang S, Pan B, Zhang W, Lv L. Hydrous ferric oxide-resin nanocomposites of tunable structure for arsenite removal: effect of the host pore structure. J Hazard Mater. 2011;198:241-6.
[29] Roghani M, Nakhli SAA, Aghajani M, Rostami MH, Borghei SM. Adsorption and oxidation study on arsenite removal from aqueous solutions by polyaniline/polyvinyl alcohol composite. J Water Process Eng. 2016;14:101-7.
[30] Huang YH, Shih YJ, Cheng FJ. Novel $KMnO_4$-modified iron oxide for effective arsenite removal. J Hazard Mater. 2011;198:1-6.
[31] Chen J, Wang J, Zhang G, Wu Q, Wang D, Facile fabrication of nanostructured cerium-manganese binary oxide for enhanced arsenite removal from water. Chem Eng J. 2018;334:1518-26.
[32] Yu Y, Zhang C, Yang L, Chen JP. Cerium oxide modified activated carbon as an efficient and effective adsorbent for the rapid uptake of arsenate and arsenite: material development and study of performance and mechanisms. Chem Eng J. 2017;315:630-8.
[33] Dahle JT, Arai Y. Environmental geochemistry of cerium: applications and toxicology of cerium oxide nanoparticles. Int J Environ Res Public Health. 2015;12(2):1253-78.
[34] Basu T, Ghosh UC. Nano-structured iron(III)-cerium(IV) mixed oxide: synthesis, characterization and arsenic sorption kinetics in the presence of co-existing ions aiming to apply for high arsenic groundwater treatment. Appl Surf Sci. 2013;283:471-81.
[35] Harish BM, Rajeeva MP, Chaturmukha VS, Suresha S, Jayanna HS, Yallappa S, et al. Influence of zinc on the structural and electrical properties of cerium oxide nanoparticles. Mater Today: Proc. 2018;5(1):3070-7.
[36] Mullins DR. The surface chemistry of cerium oxide. Surf Sci Rep. 2015;70(1):42-85.